Metallization of a Lightly Doped Emitter With Different Industrial Silver Pastes: Performance and Microscopy Analysis

Pablo Ferrada, Carlos Portillo, Valeria del Campo, Enrique Cabrera, Dominik Rudolph, Miguel Ponce Bustos, Marcelo Javier Kogan, and Radovan Kopecek

***Abstract*—Ensuring high-quality front contacts in terms of low contact and line resistance while keeping the recombination losses low in p-type silicon solar cells has been challenging for the development of silver pastes. In this work, three silver pastes were used to create a contact on a lightly doped emitter of 90 Ω/sq, produced in a tube furnace by $POCl_3$ diffusion, with an electrically active phosphorus surface concentration of 8×10^{19} cm^{-3}. The peak firing temperature (T_{peak}) and belt speed (v_{belt}) of the firing step were varied to study how the silver pastes performed. No shunting was produced after firing as pseudo fill factor exceeded 83%. Efficiencies up to 19% were measured. When firing at higher v_{belt}, a higher T_{peak} permitted higher efficiencies due to better sintering and contact formation as well as a better passivation. A selective etching procedure was applied in order to investigate the contact interface. It was found that contact imprints were preferably located at pyramid tips for all groups. The paste producing larger and deeper contact imprints led to the lowest contact resistance (4 mΩcm^2) but higher line resistance (0.46 Ω/cm) and higher saturation current density (30 fA/cm^2 above) compared with the other two pastes.**

***Index Terms*—Firing, metallization, photovoltaic cells, scanning electron microscopy, silicon, silver.**

I. Introduction

THE metallization of silver (Ag) and aluminum (Al) is a critical step within crystalline silicon (c-Si) solar cell processing. By February 2016, silver represented 7% of the nonsilicon price and one of the most expensive materials for fabrication [1]. Silver price and continuous growth of Ag consumption by PV has produced that a reduction of the metalized area is the preferred approach instead of its immediate replacement. So far, the most used technology relies on screen-printing (SP) of Ag and Al containing pastes [2]. The development of Ag pastes can contribute to the further increase of solar cell efficiency, involving the change in paste composition for best performance. Some of the advantages of this technique are the high degree of industrialization, reliability, and cost-effectiveness. This approach exhibits, however, challenges for solar cell performance. Reaching very low contact resistances, creating minimal shadowing, and producing low recombination losses are some of them. The series (R_{ser}) and shunt resistance (R_{shunt}), ideality factor (n), and the saturation current density (J_{02}) are the parameters affecting the fill factor (FF), and thus, the efficiency (η) of a solar cell [3].

Since cost reduction and high performance are pursued, the reduction of silver paste use for the front side contact is one approach for success. It can be achieved in the short term by printing narrow fingers, while ensuring a good contact quality. With regard to the paste components, the replacement of lead, due to hazardousness and restrictions (RoHS), has given impulse to further paste modifications. In the long term, other metals such as copper could be used as an alternative solution. However, the optimization of the silver paste is still been carried out delaying the full implementation of copper.

Standard p-type Si solar cells face the compromise of exhibiting a high doping concentration for ensuring a low contact resistance and, a low doping, to obtain high V_{oc} due to less recombination and high J_{sc} values due to a good blue response. This combination can be addressed by the implementation of a selective emitter structure [4], which consists of a higher doping concentration beneath the metallization grid and a lower doping level in the blue areas. Nevertheless, implementing a homogeneous emitter is attractive since pastes for c-Si solar cells can be further developed. One direction is the metallization of emitters with low doping concentration. One of the remarkable improvements of the Ag paste is to produce high-quality contacts on lightly doped emitters (LDE) [5]. Contacting LDE with decreasing lower P surface concentrations is essential to minimize surface recombination and to enable higher solar cell efficiencies.

In this work, a new emitter profile has been implemented to study how three different commercial Ag pastes perform on an

Manuscript received January 13, 2017; accepted February 20, 2017. Date of publication March 13, 2017; date of current version April 19, 2017. This work was supported in part by FONDECYT under Grant 3160190, in part by CONICYT/FONDAP "Solar Energy Research Center" under Grant 15110019, and in part by BMBF Solar Collaboration between Chile and Deutschland (Solar Child) under Grant 01DN14005.

P. Ferrada and C. Portillo are with the Centro de Desarrollo Energético Antofagasta, Universidad de Antofagasta, Antofagasta #0601, Chile (e-mail: pablo.ferrada@uantof.cl; carlos.portillo@uantof.cl).

V. del Campo is with the Department of Physics, Universidad Técnica Federico Santa María, Valparaiso 1680, Chile (e-mail: valeria.delcampo@usm.cl).

E. Cabrera, D. Rudolph, and R. Kopecek are with the International Solar Energy Research Center (ISC Konstanz), Konstanz D-78467, Germany (e-mail: enrique.cabrera@isc-konstanz.de; dominik.rudolph@isc-konstanz.de; radovan.kopecek@isc-konstanz.de).

M. P. Bustos was with the Universidad de Chile at Marcelo Kogan's group (e-mail: mponcebustos@gmail.com).

M. J. Kogan is with the Universidad de Chile, Av. Santos Dumont 964 Independencia, Santiago de Chile (e-mail: mkogan@ciq.uchile.cl).

Color versions of one or more of the figures in this paper are available online at http://ieeexplore.ieee.org.

Digital Object Identifier 10.1109/JPHOTOV.2017.2673663

LDE. The pastes were design to lead to low contact resistances on such emitters. The used emitter was produced by $POCl_3$ diffusion (P diffusion) resulting in a very thin phosphorus silicate glass (PSG). After the metallization of the Ag pastes, a firing step with varying peak firing temperature ($T_{\rm peak}$) and belt speed ($v_{\rm belt}$) followed. Characterization consisted of microscopy studies of selected samples and the measurement of the solar cell performance. The details are found in Section IV (Materials and Methods). The experiment is based on the hypothesis of producing high efficiency after metallizing an LDE.

A. Ag Paste

The Ag paste is composed of organic and inorganic components. Organics are burned off during the firing step leaving an inorganic layer. The inorganic layer contains Ag powder and metal-oxide glass frit. The glass frit is usually composed of SiO_2, PbO, and B_2O_3 [6]. While a frit such as PbO reduces the melting point supporting the etching of SiN_x during the firing step, B_2O_3 increases the chemical stability of the glass system. Indeed, B_2O_3 and PbO can reduce the viscosity of glass [7]. The glass frit chemistry of the paste will determine melting characteristics during firing step [6]. There are two ways by which Ag paste can penetrate this layer during the firing step. First, PbO oxidizes SiNx producing Pb, SiO_2 and setting N_2 free. Second, Ag dissolves as Ag_2O etching SiN_x and producing SiO_2, Ag, and N_2 [8]. The liquid phase obtained from the molten glass is the basis for the oxidation–reduction resulting in nano- and microprecipitates in the contact interface [9]. Previously, it was established that Ag crystallites can be formed without the support of liquid Pb and that the higher content of PbO increases the reactivity [10]. A fundamental study [11] reports that the glass frit with its transition temperature (T_g) plays a critical role in the contact formation. T_g is the temperature below which the glass frit becomes hard and brittle. In that work, it was found that a high T_g results in thinner glass between Ag bulk and the n-type Si. Moreover, if a high T_g glass frit crystallizes fast after SiN_x etch, it results in smaller Ag crystallites at the contact interface. This small Ag crystallite precipitation can be beneficial due to the lower current density (J_{02}) and higher $V_{\rm oc}$ [11].

After the firing process is complete, the implementation of the original paste leads to a contact structure in which the following components are found: An interfacial glass layer, pyramidal Ag crystallites penetrating Si emitter, metal and Si precipitates, and spherical Ag colloids in the glass. As a result, different current paths are possible. The final structures in the contact interface depend on the chemistry of the paste, processing parameters, and crystal orientation of the Si surfaces [12]. According to [13], the necessity of two models to explain the current path between n-type Si and the Ag bulk arises from the fact that two surface orientations of Si, namely <100> and <111>, lead to different crystallite shapes.

B. Current Transport Models

Research in the field of metallization of Si solar cells has resulted in two main models explaining the current conduction from n-type Si emitter and the Ag bulk. First, the current path is given by the charge flow through Ag crystallites grown into Si emitter, in direct contact with Ag finger or separated by a thin glass layer [5], [14], [15]. Second, the current path is given by a multistep tunneling into the Ag finger across nano-Ag colloids in a thin glass layer close to the Si emitter [16], [17]. There is evidence that these two current transport models can actually coexist, as both nanocolloids and Ag crystallite precipitation were found [18].

C. Phosphorus and Contact Formation

The study and understanding of P-diffusion and PSG can be relevant since depending on this process step, excess P doping or electrically inactive P atoms exist in Si lattice. It has been established that excess inactive P atoms in the Si lattice can produce strain and Si bond weakening, supporting the nucleation and growth of Ag crystallites [19]. Quantitatively, it was found that the density of Ag crystallites is proportional to the electrically inactive P and independent on $R_{\rm sheet}$. Using a silver paste, Ag crystallite density was independent of emitter doping, but the Ag crystallite size increased by increasing the thickness of the dead layer (i.e., more electrically inactive P). This outcome is crucial since the decrease in contact resistivity correlates with the increasing density of Ag crystallites. Conversely, a high concentration of electrically inactive P atoms can increase the size of Ag crystallites inducing recombination losses expressed as $V_{\rm oc}$ drop due to a deeper metal growth and penetration across the p-n junction. Fundamental studies regarding $V_{\rm oc}$ drop due to phosphorus precipitation are found in [20]. Furthermore, the presence of glass-free regions is required for direct contacts and depends on the paste chemistry, surface texture, and not on emitter. Investigations regarding the role and existence of direct contacts were shown in [21]. It is pointed out that direct contacts play the major role while supporting the current transport between the n-type silicon and Ag bulk.

D. Contacting LDE

In order to produce an electrical contact on an LDE with a low P surface concentration, Ag pastes can contain other oxides such as ZnO, Al_2O_3, P_2O_5, CeO_2, TiO_2, or MgO, as well as alkali elements like Na, Li, K, and fluorides such as AlF_3 and BiF_3 [22]. These compounds can be used to control the etching process [5], [23], [24]. Moreover, varying the Ag particle size from 100 nm to 10 μm and the shape such as flake or spherical, the features of the contact interface can be adjusted. The use of a paste with larger Ag particle size can lead to more dissolution of Ag in the glass, resulting in larger Ag crystallites. However, as mentioned, too big Ag crystallites can potentially produce shunting in the p-n junction. It was founded that small spherical Ag particles can provide higher FF and $V_{\rm oc}$ values [5].

An investigation of 2013 using industrial Ag pastes showed absolute efficiency gains up to 0.3%, reaching a maximum $\eta = 18.6\%$ on p-type Cz monocrystalline Si solar cells. Those solar cells exhibited a high density of Ag crystallites with a very narrow interfacial glass layer enabling an electrical contact on an LDE. It was found that bigger and deeper Ag crystallites

with a thin and discontinuous interfacial layer led to the higher η values. This result was supported by the existence of direct contact between the Ag crystallites grown in the n-type Si emitter and the Ag bulk. The contact quality was ensured for surface concentration as low as $1.7 \times 10^{20}\,\mathrm{cm}^{-3}$ [25]. According to ITRPV 2016, the state-of-the-art efficiency for CZ p-type Al-back surface field (BSF) solar cells was 19.5% in 2015, 19.7% in 2016, and expected to be above 20% in 2020 [1].

The dominant current transport mechanisms on LDE may differ from that on highly doped emitters (HDE). It was reported that for LDE, only high T_{peak} values have enabled a low contact resistance, based on the Ag crystallite mechanism. For HDE, the two current transport mechanisms were found to be possible, namely Ag crystallites and nano-Ag colloids at low T_{peak}. Consequently, both doping profile and T_{peak} play a big role in defining optimal firing conditions.

An "optimal firing" was defined as the condition, where a few Ag crystallites and Ag colloids within an ultrathin interfacial glass film are found, leading to the maximum achievable FF of a c-Si solar cell [18]. When FF deviates from the optimal value, due to a low density of Ag crystallite and nonexistence of nano-Ag colloids, an "overfiring condition" was defined [26].

Based on the findings described, it is possible to establish that the existence of nano-Ag colloids and a thin glass layer may not be enough to ensure a low contact resistance on LDE.

II. Materials and Methods

Three Ag pastes were screen printed on a 90 Ω/sq emitter, which was created by $POCl_3$ diffusion resulting in an emitter profile with a very narrow dead layer. The purpose was to reach highest solar cell performance after SP and firing [27]. Each emitter/silver paste combination has an optimal firing condition, where best efficiency has to be found. In the following, the procedure is described.

A. Solar Cell Processing and Characterization

Solar cells were processed starting with p-type boron doped monocrystalline Si wafers of $15.6 \times 15.6\ \mathrm{cm}^2$ size, 1.5–2 Ωcm resistivity, and 200 μm thickness. A wet-chemical process was used to remove the saw damage and to texture the Si wafer surface. This step was achieved by an alkaline etching in a RENA batch composed of potassium hydroxide mixed with isopropyl alcohol at 80 °C. A cleaning step before p-n junction formation in RENA indus process consisted of a deionized water (DW) bath until 1.5 MΩ was measured in the water, an HCl bath at 3% and room temperature (RT) for 5 min, a DW bath until 1.5 MΩ was obtained, HF bath at 2% and RT for 2 min and DI bath until 1.5 MΩ was achieved. Wafers were blown with N_2 and dried for 12 min at 110 °C in N_2 ambient.

After texturing and cleaning, $POCl_3$ diffusion, plasma enhanced chemical vapor deposition (PECVD) SiN_x passivation/antireflexion deposition, SP, and cofiring followed. P diffusion led to the emitter profile shown in Fig. 1. PECVD standard recipe was used for all wafers. The metallization consisted of the SP of three different industrial Ag pastes using a Baccini screen-printer. Thus G1, G2, and G3 were defined according

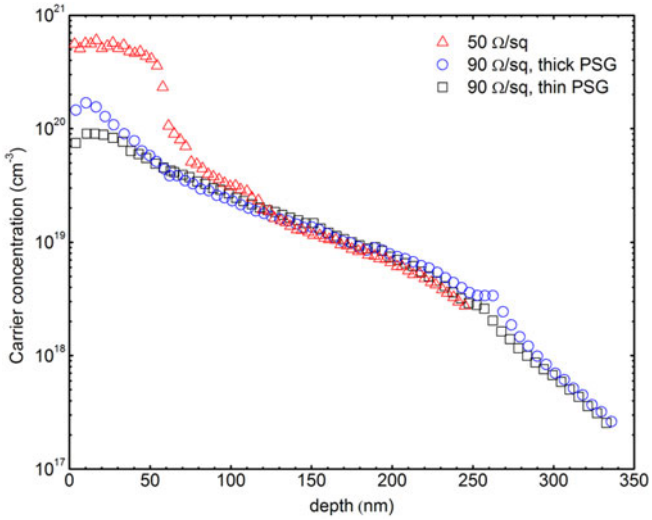

Fig. 1. Emitter profiles measured by electrochemical capacitance voltage.

TABLE I
T_{peak} AND v_{belt} USED FOR FIRING G1, G2, AND G3

Group	Tpeak (°C)	v_{belt} (m/ mm) [a]
G1	875, 890, 905, 910	7, 8
G2	860, 875, 890, 905, 910, 920, 930	7, 8, 9
G3	860, 875, 890, 905, 910, 920, 930	7, 8, 9

to the Ag paste used. While G1 contains silver powder in the range 80–90%, organics up to 1%, glass compounds up to 10%, Pb-glass up to 1%, and others up to 10, G2 is made up of silver between 60% and 90% and glass frit up to 3%. In the case of G3, silver powder ranges 75–100%, Pb glass is found up to 2.5%, zinc oxide is present up to 0.5%, and others up to 15%.

For the firing step, the peak firing temperature T_{peak}, and the belt speed v_{belt} were varied in a CentroTherm firing furnace. Table I shows the used T_{peak} and v_{belt} values.

Fig. 1 shows three different doping profiles for comparison. An LDE of 90 Ω/sq with a thin PSG, which was used for this work, an LDE with a thick PSG of 90 Ω/sq, and a HDE with an R_{sheet} of 50 Ω/sq. The surface concentration for each case was $7.5 \times 10^{19}\,\mathrm{cm}^{-3}$, $1.5 \times 10^{20}\,\mathrm{cm}^{-3}$, and $5.6 \times 10^{20}\,\mathrm{cm}^{-3}$.

The solar cell illuminated and dark IV characteristics were determined with a flasher from h.a.l.m. elektronik Gmbh. The device provides series and shunt resistances, pseudo fill factor (pFF), and saturation current densities (J_{01}, J_{02}). Electroluminescence (EL) was used to find optimum T_{peak} and v_{belt}. The best solar cell samples correspond to T_{peak} and v_{belt} values of 890 °C and 7 m/ mm for G1, 910 °C and 8 $\mathrm{m/mm}$ for both G2 and G3, shown in Fig. 2.

Selected solar cells of each group, according to EL, were cleaved via laser beam on the rear side and broken per hand to obtain stripes of $15.6 \times 1\ \mathrm{cm}^2$ size. The specific contact resistance (ρ_c) was determined with the transfer length method. The line resistance (R_{line}) was measured from busbar to busbar.

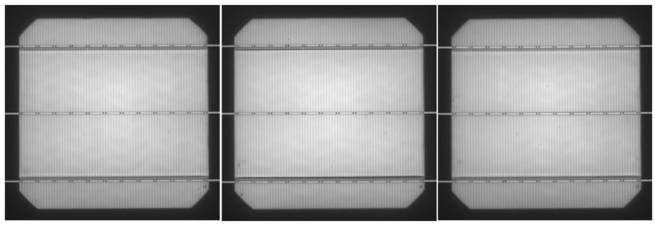

Fig. 2. Electroluminescence images for (a) G1, (b) G2, and (c) G3.

B. Sample Preparation for Scanning Electron Microscopy (SEM) Analysis

In order to perform the interface analysis of the resulting contacts, the stripes were treated with aqua regia (AR) for 1 h to remove the metal from the silver (Ag) bulk. AR bath was applied at RT consisting in 3:1 mixture of HNO_3 at 65% and HCl at 32%. Subsequently, HF bath at 5% at RT to dissolve the glass layer and a second AR step to remove the Ag crystallites formerly underneath the glass [28] were applied followed by SEM [29].

III. Results

A. Microscopy After Chemical Treatment

After applying AR for 1 h, Ag fingers were completely removed for G1 and G2. However, some Ag residues remained at G2. Even after 1 h AR application, Ag fingers were not completely removed for G3. For all groups, the glass covered the pyramid tips and a thick inhomogeneous glass layer is seen on the surface [see Fig. 3(a)–(c)]. Some crystallites at the pyramid tips are also distinguishable.

Sequentially after applying an HF step [see Fig. 3(d)–(f)], Ag crystallites seem to be at the pyramid tips for G1 with clusters of Ag particles along the edges. These clusters do not contain crystallites necessarily. G2 exhibits a numerous amount of large Ag crystallites at pyramid tips, around the tip, and at the edges. For this group (G2), large Ag clusters of sintered particles at different positions such as edges at mid height of the pyramid and valleys were found. In the case of G3, Ag imprints are already found after HF application. It seems to be fewer amounts of Ag residues compared to G1 and G2. It could also mean that the glass layer at the pyramid tips is thinner than in the case of G1 and G2 or some of the tips are completely free of glass, which means that the Ag at the tips was already etched after the first AR etching step. This observation agrees with the lower ρ_c of G3 ($4\ \mathrm{m\Omega cm^2}$).

After applying a second AR step [see Fig. 3(g)–(i)], small contact imprints at the pyramid tips of very defined geometries (triangles) were found for G1. There were small fractions of Ag rest left for this group. G2 shows small contact imprints without a well-defined geometry as for G1. There are large amount of Ag rests in spite of two AR steps of 1 h each. Finally, for G3, large contact imprints at the pyramid tips were observed. They seem to be deeper than for G1 and G2. There were small imprints at the edges and small fractions of Ag rest left. For all groups, contact imprints were found at the pyramid tips and edges close to the pyramid tip.

When selective etching is applied to remove the Ag finger (Ag bulk), the crystallites, which were located at the pyramid tips, are taken away as well. This effect is obtained since no glass layer protects the Ag crystallites against the etching. The glass exists more abundantly in the valleys between pyramids and Ag crystallites preferably grow at the pyramid tips. It is at these locations (the tips) where direct contacts are found. In [21], it was quantitatively demonstrated that Ag crystallites located at the pyramid tips support the current conduction between the Si emitter and Ag bulk to a larger extent. Applying liquid conductive silver paint to Ag crystallite exposed interface, low ρ_c were measured. These values were as low as $1.5\ \mathrm{m\Omega cm^2}$ for the case when only Ag crystallites protected under the glass remained and less than $1\ \mathrm{m\Omega cm^2}$ for the case when all the Ag crystallites grown into the n-type Si remained. Thus, from these results, only $0.5\ \mathrm{m\Omega cm^2}$ is roughly the contribution of Ag crystallites located at the tips of pyramids to the ρ_c value due to Ag crystallites located from tip to bottom of Si pyramids.

B. Line and Contact Resistance

The line resistance for G1 reached the local minimum at 890 °C and 7 m/min ($R_{\mathrm{line}} = 0.42\,\Omega/\mathrm{cm}$). R_{line} can be even smaller, however, at a higher temperature (910 °C). G2 and G3 exhibit a linear behavior for which a higher temperature leads to lower R_{line} values. The general tendency is that, for a constant v_{belt}, R_{line} decreases as T_{peak} increases. For a given T_{peak} value (e.g., 910 °C), R_{line} of G2 and G3 obtained with $v_{\mathrm{belt}} = 9$ m/min are shifted to higher values compared to those achieved $v_{\mathrm{belt}} = 7$ m/min. At 8 m/mm, R_{line} still is decreased as T_{peak} increases.

Samples from G1, G2, and G3 resulted in specific contact resistance (ρ_c) values of $5.3 \pm 1.5\ \mathrm{m\Omega cm^2}$, $4.1 \pm 1.1\ \mathrm{m\Omega cm^2}$, and $4.1 \pm 2.1\ \mathrm{m\Omega cm^2}$, respectively. The deviation indicates that in principle, all pastes can potentially reach ρ_c values below $5\ \mathrm{m\Omega cm^2}$. These values represent the macroscopic behavior of the Ag/n-type Si contact. A microscopic characterization has shown that ρ_c values of Ag crystallites range between 0.2 and $0.4\ \mu\mathrm{\Omega cm^2}$ [14], [15].

C. IV Measurements

Fig. 4 shows the IV measurements with regard to the peak firing temperature, belt speed, and group. The FF improved for all groups as T_{peak} increased. For G1 and G2, same levels for the FF were found (maximum of 78.2% in average for the whole T_{peak} range used). For G3, the low temperature range suggests no complete sintering, correlating with the R_{line} values. These R_{line} values explain the lower FF of G3 in comparison with the FF of G1 and G2. At 910 °C, the FF started to reach a maximum. At 8 m/min and 910 °C, FF was slightly higher than at $7\ \mathrm{m/min}$ for G2 and G3. The v_{belt} had more impact in G3 as the higher $v_{\mathrm{belt}} = 9$ m/ mm led to 77.65%, which is much below its maximum FF. However, at 9 m/ mm, an increase of T_{peak} resulted in the maximum FF for G3. In the case of J_{sc}, a

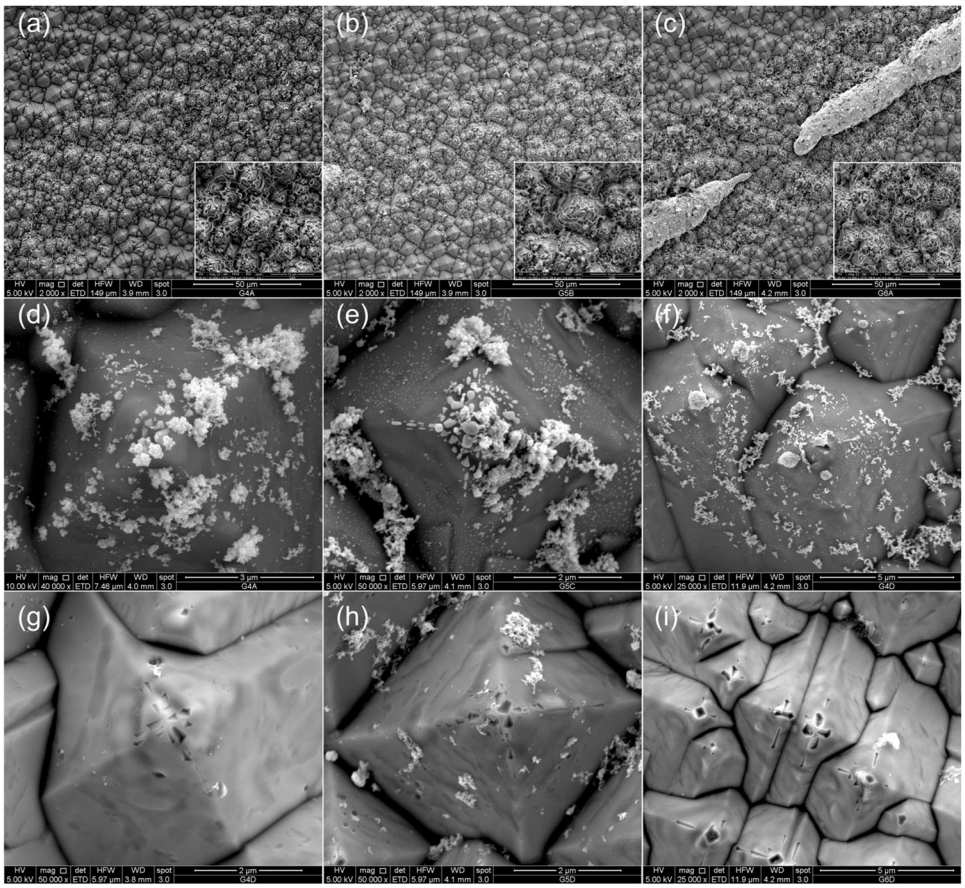

Fig. 3. SEM images (a), (b), and (c) are after AR treatment for groups G1, G2, and G3, respectively. The SEM images (d), (e), and (f) are after AR and HF treatments for groups G1, G2, and G3, respectively. The SEM images (g), (h), and (i) are after AR, HF, and AR treatments for groups G1, G2, and G3.

common decreasing tendency was found as T_{peak} increased for all groups. The V_{oc} curves of each group did not exhibit the same behavior with regard to T_{peak} as only G3 shows a clear optimum V_{oc} at 890 °C. For G1, V_{oc} decreased as T_{peak} increased and in this case the optimum V_{oc} and J_{sc} were at the lowest T_{peak} (875 °C). For G2, also the best V_{oc} and J_{sc} were found at the lowest T_{peak} (860 °C). For G3 at 7 m/min, lowest and highest temperature indicates, as documented in an incomplete BSF formation and an overfiring condition, respectively [27]. The belt speed of 8 m/ min at 910 °C of G2 and G3 produced a higher V_{oc} and J_{sc} value than those found at 7 m/ min. This result can be related to a reduced recombination due to a less chance of growing too big Ag crystallites and introducing traps into the bulk. Studies with regard to the V_{oc} degradation have shown a connection with the metal penetration into the silicon material. One of these investigations based on simulation came to the conclusion when metal particles penetrate close to the p-n junction, recombination via defects occur deteriorating V_{oc} [30]. Particularly, it was established that shallow emitters exhibit the largest V_{oc} drop with respect to the implied V_{oc} before metallization, whereas deep emitters result in a slower V_{oc} drop. A complete BSF formation allows for improving the quantum efficiency and thus the J_{sc}. For the FF, the deterioration can be also influenced by the diffusion of Ag particles into silicon at moderate temperatures (400–700 °C) [31].

IV. Discussion

During the firing step several phenomena occur in the solar cell.

1) H atoms introduced in the PECVD-SiNx diffuse into the bulk Si and passivate defects (more effective in mc-Si material). The emitter saturation current density (J0e) can be reduced by 45% when measuring after firing and after PECVD deposition (no fired solar cells) [28].
2) Quality of the SiN_x passivation improves.
3) The Ag contact to n-type Si is created.
4) Ag particles are sintered.
5) An Al-BSF is formed passivating the rear side of the solar cell.

Thus, the influence of T_{peak} and v_{belt} can have detrimental effects on both 1) contact quality and 2) recombination. For 1), an incomplete sintering can lead to high R_{line} values and the growing of a thick glass layer isolates the Ag bulk and Ag crystallites increasing ρ_{c}. To the recombination currents, while J_{01} corresponds to losses in the emitter and bulk, and at the front as well as the rear surface, J_{02} is associated to recombination in the space charge region (SCR). For 2), the introduction of surface states can lead to higher surface recombination velocities, the growing of too big Ag crystallites can penetrate the p-n junction reaching the SCR and resulting in higher J_{02} values,

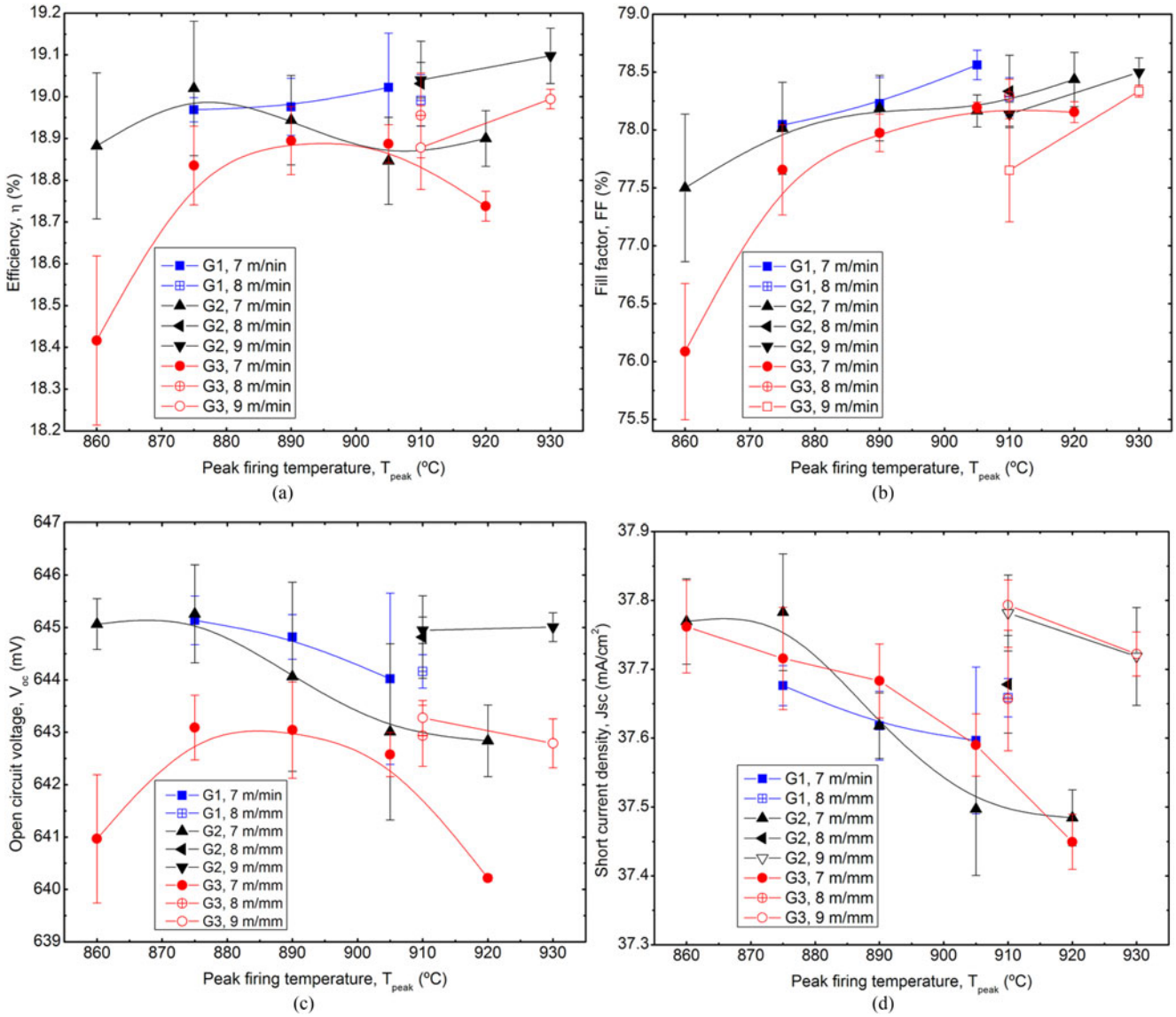

Fig. 4. IV measurements: (a) Efficiency, (b) FF, (c) $V_{\rm oc}$, and (d) FF as a function of $T_{\rm peak}$ and $v_{\rm belt}$ for G1, G2, and G3.

the partial or incomplete creation of the Al-BSF can contribute to an increase of J_{01}.

The macroscopic behavior expressed in the IV measurements can be understood by direct comparison of further performance parameters, i.e., average and standard deviation values for $R_{\rm ser}$, $R_{\rm shunt}$, $R_{\rm line}$, J_{01}, and J_{02} shown in Table II. These resistance and recombination current densities of the selected samples from G1, G2, and G3 for SEM are shown in Table III.

The effects of SP metallization and firing can materialize in three loss categories: ohmic, recombinative, and optical. From a theoretical basis, while $R_{\rm ser}$, $R_{\rm shunt}$, and J_{02} can affect the FF, J_{01} and J_{02} are related to the lowering of $V_{\rm oc}$.

According to the results shown in Table II summarizing average values, the Ag paste defining G3 resulted in the lowest FF explained by the highest $R_{\rm ser}$, which is corresponded by the highest $R_{\rm line}$, and the highest J_{02}. It was for this paste (G3) that a higher glass content was found, explaining the higher $R_{\rm line}$.

TABLE II
SUMMARY OF SOLAR CELL MEASUREMENTS FOR G1, G2, AND G3 AFTER SELECTING FIRING PARAMETERS

Group	FF (%)	$R_{\rm ser}$ (Ωcm^2)	$R_{\rm line}$ (Ω/cm)	J_{02} (nA/cm^2)
G1	78.23 ± 0.22	0.80 ± 0.04	0.42 ± 0.01	32.30 ± 1.5
G2	78.33 ± 0.33	0.77 ± 0.04	0.42 ± 0.01	32.92 ± 3.1
G3	78.29 ± 0.15	0.82 ± 0.02	0.46 ± 0.01	33.56 ± 1.7
Group	$V_{\rm oc}$ (mV)	$J_{\rm sc}$ (mA/cm^2)	J_{01} (fA/cm)	η (%)
G1	644.8 ± 0.4	37.6 ± 0.05	358.1 ± 5.7	18.98 ± 0.07
G2	644.8 ± 0.8	37.7 ± 0.07	356.9 ± 11	19.03 ± 0.10
G3	642.9 ± 0.6	37.7 ± 0.08	385.9 ± 7.1	18.96 ± 0.06

The Ag paste used for G2 led to the highest FF also supported by the lowest $R_{\rm ser}$ and $R_{\rm line}$. The resistances were more dominant than J_{02}. However, according to Table III, the sample prepared from G2 for SEM analysis exhibited the lowest J_{02}.

TABLE III
SUMMARY OF SOLAR CELL MEASUREMENTS OF PREPARED SAMPLES FROM G1, G2, AND G3

Group	FF (%)	$R_{\rm ser}$ (Ωcm^2)	$R_{\rm line}$ ($\Omega/$cm)	J_{02} (nA/cm^2)
G1	78.25	0.78	0.42	33.26
G2	78.51	0.74	0.42	31.45
G3	78.44	0.78	0.47	32.11
Group	$V_{\rm oc}$ (mV)	$J_{\rm sc}$ (mA/cm^2)	J_{01} (fA/cm)	η (%)
G1	644.6	37.7	358.0	19.00
G2	644.8	37.6	361.7	19.03
G3	642.5	37.6	398.0	18.94

The influence of Ag paste defining G3 produced a 2 mV lower $V_{\rm oc}$ with respect to G1 and G2, explained by a higher recombination. Indeed, defining $\Delta J_{01} = J_{01,\rm G3} - J_{01,\rm G2}$, the relative difference $\Delta J_{01}/J_{01,\rm G2}$ results as high as 8.2% from Table II and 10% from Table III. It means that J_{02} of G3 could be in the order of 10% higher than J_{02} of G2 supporting $\Delta V_{\rm oc} = 2$ mV when comparing $V_{\rm oc}$ of G1 or G3 with that of G2. In terms of $J_{\rm sc}$, similar photo current were obtained with G1, G2, and G3.

V. CONCLUSION

In view of minimizing surface recombination and enabling higher solar cell efficiencies for crystalline silicon solar cells, three industrial silver pastes were used to produce a contact on an LDE. This emitter profile exhibited a sheet resistance of 90 $\Omega/$sq and a surface concentration of 8×10^{19} cm^{-3}, created by phosphorus diffusion. According to the silver paste for the screen-printed, three groups (G1, G2, and G3) were defined and solar cells were produced. For the firing step, a wide range of peak firing temperatures ($T_{\rm peak}$) from 860 °C to 920 °C and three belt speed ($v_{\rm belt}$) values of 7, 8, and 9 m/mm were used.

The microscopy analysis on prepared samples found large and deep contact imprints, correlating with the saturation current density. This result agrees with previous evidence of the necessity of bigger and deeper Ag crystallites with a thin and discontinuous interfacial layer in order to achieve high η.

Contact imprints were preferably located at the pyramid tips for all groups. These contact locations can be a condition for producing good quality contacts on LDEs. This statement is supported since there is evidence that the main path contributing to the current transport in c-Si solar cells is via silver crystallites gown in n-type emitter in direct contact with the silver bulk.

Solar cell performance clearly showed a dependence on $T_{\rm peak}$ and $v_{\rm belt}$. While FF increased with higher $T_{\rm peak}$ and constant $v_{\rm belt}$, $J_{\rm sc}$ decreased. With a higher $v_{\rm belt}$, a higher $T_{\rm peak}$ was enabled for higher efficiencies due to better sintering and contact formation as well as a better field passivation. The pFF was above 83% for all groups indicating no shunting. However, differences in the FF and open circuit voltage ($V_{\rm oc}$) accounted for contact quality and recombination losses for each group. These values were in agreement with the series resistance ($R_{\rm ser}$) and line resistance ($R_{\rm line}$) mostly affecting the FF and the saturation current density (J_{01}) having an impact on $V_{\rm oc}$. Indeed, the high $R_{\rm ser}$ of G3 led to the lowest FF among the groups. The higher $R_{\rm ser}$ value of G3 was dominated by a higher $R_{\rm line}$. While the $V_{\rm oc}$ of G1 and G2 were similar, G3 exhibited a 2 mV lower $V_{\rm oc}$ due to the higher saturation current density (J_{01}) of G3 (up to 30 fA/cm^2 above that of G1 and G2). The $V_{\rm oc}$ was more sensitive to the Ag paste used. While G1 and G2 led to a decreasing $V_{\rm oc}$ tendency with $T_{\rm peak}$ at constant $v_{\rm belt}$, G3 showed a clear optimum. As a result, efficiencies of each group followed this pattern.

Overall, efficiencies up to 19% with an FF of 78.6% were achieved on an LDE of 90 $\Omega/$sq and a surface concentration of 8×10^{19} cm^{-3}.

REFERENCES

[1] International Technology Roadmap for Photovoltaic, 2016.

[2] G. Schubert, G. Beaucarne, and J. Hoornstra, "The future of metallization—Forecast of the experts of the 5th metallization workshop," *Energy Procedia*, vol. 67, pp. 13–19, 2015. doi:10.1016/j.egypro.2015.03.283.

[3] A. Ebong, "Metallization of crystalline silicon solar cells: A review," in *Proc. 9th Int. Conf. High Capacity Opt. Netw. Enabling Technol.*, Istanbul, Turkey, Dec. 2012, pp. 102–109. doi:10.1109/HONET.2012.6421444.

[4] M. Z. Rahman, "Status of selective emitters for p-type c-Si solar cells," *Opt. Photon. J.*, vol. 2, pp. 129–134, 2012. doi:10.4236/opj.2012.22018.

[5] M. M. Hilali *et al.*, "Understanding and development of manufacturable screen-printed contacts on high sheet-resistance emitters for low-cost silicon solar cells," *J. Electrochem. Soc.*, vol. 152, no. 10, pp. G742–G749, 2005. doi:10.1149/1.2001507.

[6] M. M Hilali and A. Rohatgi, "A review and understanding of screen-printed contacts and selective–emitter formation," in *Proc. 14th Workshop Crystalline Silicon Sol. Cells Modules*, Winter Park, CO, USA, Aug. 2004, pp. 109–116.

[7] Y. Zhang, Y. Yang, J. Zheng, W. Hua, and G. Chen, "Thermal properties of glass frit and effects on Si solar cells," *Mater. Chem. Phys.*, vol. 114, pp. 319–322, 2009. doi: 10.1016/j.matchemphys.2008.09.011.

[8] J. D. Fields *et al.*, "The formation mechanism for printed silver-contacts for silicon solar cells," *Nature Commun.*, vol. 7, 2016, Art. no. 11143. doi:10.1038/ncomms11143.

[9] M. Eberstein *et al.*, "In-situ observations of glass frit related effects during the front side paste contact formation," in *Proc. IEEE 40th Photovolt. Spec. Conf.*, Denver, CO, USA, Jun. 2014, pp. 3462–3469. doi:10.1109/PVSC.2014.6925678.

[10] K. K. Hong *et al.*, "Mechanism for the formation of Ag crystallites in the Ag thick-film contacts of crystalline Si solar cells," *Sol. Energy Mater. Sol. Cells*, vol. 93, pp. 898–904, 2009. [Online]. Available: http://dx.doi.org/10.1016/j.solmat.2008.10.021

[11] M. M. Hilali *et al.*, "Effect of glass frit chemistry on the physical and electrical properties of thick-film ag contacts for Si solar cells," *J. Electron Mater.*, vol. 35, no. 11, pp. 2041–2047, 2006. doi:10.1007/s11664-006-0311-x.

[12] A. Khanna *et al.*, "Influence of random pyramid surface texture on silver screen-printed contact formation for mono crystalline silicon wafer solar cells," *Sol. Energy Mater. Sol. Cells.*, vol. 132, pp. 589–596, 2015. [Online]. Available: http://dx.doi.org/10.1016/j.solmat.2014.10.018

[13] P. Kumar, M. Pfeffer, B. Willsch, and O. Eibl, "Contact formation of front side metallization in p-type, single crystalline Si solar cells: Microstructure, temperature dependent series resistance and percolation model," *Sol. Energy Mater. Sol. Cells*, vol. 145, pp. 358–367, 2016. Online]. Available: http://dx.doi.org/10.1016/j.solmat.2015.10.042.

[14] C. Ballif, D. M. Huljic, G. Willeke, and A. Hessler-Wyser, "Silver thick-film contacts on highly doped n-type silicon emitters: Structural and electronic properties of the interface," *Appl. Phys. Lett.*, vol. 82, no. 12, pp. 1878–1880, 2003. doi:10.1063/1.1562338.

[15] S. Kontermann, R. Preu, and G. Willeke, "Calculating the specific contact resistance from the nanostructure at the interface of silver thick film contacts on n-type silicon," *Appl. Phys. Lett.*, vol. 99, 2011, Art. no. 111905. [Online]. Available: http://dx.doi.org/10.1063/1.3635383

[16] Z. Li, L. Liang, and L. Cheng, "Electron microscopy study of front-side Ag contact in crystalline Si solar cells," *J. Appl. Phys.*, vol. 105, no. 6, 2009, Art. no. 066102. [Online]. Available: http://dx.doi.org/10.1063/1.3086663

[17] S. B. Cho, H. S. Kim, and J. Y. Huh, "Mechanism underlying the beneficial effect of forming gas annealing on screen-printed Ag contacts of crystalline Si solar cells," *Acta Mater.*, vol. 70, pp. 1–7, 2014. [Online]. Available:http://dx.doi.org/10.1016/j.actamat.2014.02.023

[18] Z. G. Li *et al.*, "Microstructural comparison of silicon solar cells' front-side Ag contact and evolution of current conduction mechanism," *J. Appl. Phys.*, vol. 110, 2011, Art. no. 074304. [Online]. Available: http://dx.doi.org/10.1063/1.3642956
[19] E. Cabrera *et al.*, "Impact of excess phosphorus doping and Si crystalline defects on Ag crystallite nucleation and growth in silver screen-printed Si solar cells," *Prog. Photovolt. Res. Appl.*, vol. 23, pp. 367–375, 2015. doi:10.1002/pip.2440.
[20] P. Ostoja, S. Guerri, P. Negrini, and S. Solmi, "The effects of phosphorus precipitation on the open circuit voltage in n+p silicon solar cells," *Solar Cells*, vol. 11, no. 1, pp. 1–12, 1984. doi:10.1016/0379-6787(84)90114-5.
[21] E. Cabrera *et al.*, "Experimental evidence of direct contact formation for the current transport in silver thick film metallized silicon emitters," *J Appl. Phys.*, vol. 110, 2011, Art. no. 114511. [Online]. Available: http://dx.doi.org/10.1063/1.3665718
[22] G. Laudisio, R. J. S. Young, P. J. Willmot, and K. W. Hang, "Metal pastes and use thereof in the production of silicon solar cells," U.S. Patent 0240124 A1, 2011.
[23] H. A. Bethe, *Theory of the Boundary Layer of Crystal Rectifiers*. Cambridge, MA, USA: Radiation Laboratory, Massachusetts Inst. Technol., 1942, pp. 43–12.
[24] S. Kontermann, "Characterization and modeling of contacting crystalline silicon solar cells," Ph.D. dissertation, Univ. Konstanz, Konstanz, Germany, 2009.
[25] V. Shanmugam *et al.*, "Electrical and microstructural analysis of contact formation on lightly doped phosphorus emitters using thick-film ag screen printing pastes," *IEEE J. Photovolt.*, vol. 4, no. 1, pp. 168–174, Jan. 2014.
[26] I. B. Cooper *et al.*, "Investigation of the mechanism resulting in low resistance ag thick-film contact to si solar cells in the context of emitter doping density and contact firing for current-generation ag paste," *IEEE J. Photovolt.*, vol. 4, no. 1, pp. 134–141, Jan. 2014.
[27] I. B. Cooper *et al.*, "Understanding and use of IR belt furnace for rapid thermal firing of screen printed contacts to Si solar cells," *IEEE Device Lett.*, vol. 31, no. 5, pp. 461–463, May 2010.
[28] G. Schubert, "Thick film metallisation of crystalline silicon solar cells," Ph.D. dissertation, Univ. Konstanz, Konstanz, Germany, 2006.
[29] P. Ferrada *et al.*, "Selective chemical etching for studying the front side contact in thick film screen printed crystalline p-type silicon solar cells," *J. Chilean Chem.*, vol. 2, pp. 2905–2910, 2015. [Online]. Available: http://dx.doi.org/10.4067/S0717-97072015000200009
[30] L. J. Koduvelikulathu *et al.*, "Metallization and firing process impact on V_{oc}—A simulation study," in *Proc. 27th Eur. Photovolt. Solar Energy Conf. Exhib.*, Frankfurt, Germany, 2012, pp. 1432–1434. doi:10.4229/27thEUPVSEC2012-2BV.5.33.
[31] L. Chen, Y. Zeng, P. Nyugen, and T. L. Alford, "Silver diffusion and defect formation in Si (111) substrate at elevated temperatures," *Mater. Chem. Phys.*, vol. 76, no. 3, pp. 224–227, 2002. doi:10.1016/S0254-0584(01)00529-6.

Pablo Ferrada received the Dipl.-Ing. degree in electrical engineering in the field of control theory from Universidad de Santiago, Santiago, Chile, in 2007 and the Ph.D. degree in applied physics in the field of crystalline silicon solar cells from the University of Konstanz, Konstanz, Germany, in 2012. He completed his diploma thesis at the Institute of Automatic Control, RWTH-University, Aachen, Germany.

He worked in the field of silicon solar cells at the International Solar Energy Research Center Konstanz. Currently, he works as a Postdoctoral Researcher at the Antofagasta Center for Energetic Development, University of Antofagasta, Antofagasta, Chile, and a Guest Researcher at the Solar Energy Research Center Chile.

Carlos Portillo received the Dipl. Ing. degree in electrical engineering in the field of control theory from Universidad Católica del Norte, Antofagasta, Chile, in 2007 and the Ph.D. degree in applied physics in the field of crystalline silicon solar cells from the Faculty of Physics and Mathematics, University of Chile, Santiago, Chile, in 2012.

He is currently an Associate Professor in the Faculty of Engineering, University of Antofagasta and a Researcher at the Center for energy development in the area of PV materials and specialist in theoretical solid-state spectroscopy.

Valeria del Campo received the Ph.D. degree in physics from Pontificia Universidad Católica de Chile, Santiago, Chile, in 2009.

She is currently a Researcher with the Universidad Técnica Federico Santa María, Valaparaiso, Chile. Her research area is surface science, in which her main lines are graphene and carbon materials, self-assembled monolayers, PV cells, and characterization and applications of nanomaterials.

Enrique Cabrera received the Dipl.-Ing. (Hons.) degree in electrical engineering and electrical power systems from the Universidad de Santiago de Chile, Santiago, Chile, in 2008, and the Ph.D. degree in physics in the field of metallization of silicon solar cells from the International Solar Energy Research Center Konstanz in cooperation with the University of Konstanz, Konstanz, Germany. As a part of his studies, he spent one year at the RWTH Aachen University, Aachen, Germany, as a DAAD scholarship holder.

He is currently working as a Researcher and a Project Coordinator in several EU projects and supporting R&D and cooperation projects in Chile.

Dominik Rudolph studied microsystems engineering in Freiburg. He received the German Diploma degree in April 2008, focusing on the subject "Laser-Induced Metallization of Silicon Solar Cells from an Aqueous Electrolyte" from Fraunhofer Institute for Solar Energy Systems, Freiburg, Germany.

Since February 2009, he has been working as a scientist, responsible for the metallization processes and quality control.

Miguel Ponce Bustos, photograph and biography not available at the time of publication.

Marcelo Javier Kogan received the Ph.D. degree in organic chemistry from the University of Buenos Aires, Buenos Aires, Argentina, in 1996.

He is a Professor with the Department of Pharmacology and Toxicology, School of Pharmacy, University of Chile, Santiago, Chile, and a Principal Investigator at the Advanced Center for Chronic Diseases. He is the Director of the Laboratory of Nanomedicine and Nanotheranostics at this center. He is a Biochemist and a Pharmacist with the University of Buenos Aires. His interest is centered on applications of nanobiomaterials in biomedicine for diagnosis and treatment of conformational diseases.

Radovan Kopecek received the Dipl. Phys. degree from the University of Stuttgart, Stuttgart, Germany, in 1998, in the field of superconductive fullerides, and the Ph.D. degree in applied physics from University of Konstanz in the field of thin film silicon solar cells at Prof. Bucher's group, in 2002.

One of the founders of ISC Konstanz, he is since 2007 the Leader of the advanced solar cells department dealing with several European and national research projects in the field of silicon feedstock and solar cell development. He has been teaching the basics of PV at DHBW Friedrichshafen since 2012. Since 2016, he has been in the board of directors at EUREC.